Quasi-two-dimensional behavior of 112-type iron-based superconductors

D. Sóñora,[1] C. Carballeira,[1] J. J. Ponte,[2] Tao Xie,[3,4] Huiqian Luo,[3] Shiliang Li,[3,4,5] and J. Mosqueira[1,*]

[1]*LBTS, Departamento de Física de Partículas, Universidade de Santiago de Compostela, E-15782 Santiago de Compostela, Spain*
[2]*Unidade de Magnetosusceptibilidade, RIAIDT, Universidade de Santiago de Compostela, E-15782 Santiago de Compostela, Spain*
[3]*Beijing National Laboratory for Condensed Matter Physics, Institute of Physics, Chinese Academy of Sciences, Beijing 100190, China*
[4]*University of Chinese Academy of Sciences, Beijing 100190, China*
[5]*Collaborative Innovation Center of Quantum Matter, Beijing 100190, China*

(Received 6 February 2017; revised manuscript received 7 June 2017; published 24 July 2017)

Fluctuation magnetoconductivity and magnetization above the superconducting transition temperature (T_c) are measured on the recently discovered 112 family of iron-based superconductors (IBS), $Ca_{1-x}La_xFe_{1-y}Ni_yAs_2$, which presents an extra As-As chain spacer-layer. The analysis in terms of a generalization of the Lawrence-Doniach approach to finite applied magnetic fields indicates that these compounds are among the most anisotropic IBS (γ up to $\sim$30) and provides compelling evidence of a *quasi*-two-dimensional behavior for doping levels near the optimal one.

DOI: 10.1103/PhysRevB.96.014516

I. INTRODUCTION

All families of iron-based superconductors (IBS) share a similar crystal structure consisting of FeAs superconducting layers separated by spacer layers that determine many of their properties [1]. Recently a new class of IBS (the 112 family) has been discovered based on the compound $Ca_{1-x}La_xFeAs_2$ [2] that has raised great interest [3–10]. In addition to the Ca/La spacer layer, these compounds present an extra spacer layer with zigzag As chains that introduces an additional electron band near the Fermi level [6,9]. In agreement with a previous theoretical study [7], this band presents a Dirac-cone structure [10], which led to the recent proposal that these compounds may behave below T_c as natural topological superconductors [7,10]. The extra As layer also increases significantly the distance between the superconducting FeAs layers (up to $\sim$10.3 Å) as compared with the most studied IBS families. This could strongly enhance the superconducting anisotropy and even affect the spatial dimensionality of the superconducting order parameter, at present an open issue in IBS. For instance, compounds with smaller FeAs layer interdistances were claimed to present two-dimensional (2D) characteristics (e.g., LiFeAs [11,12], $FeSe_{1-x}Te_x$ [13], and SmFeAsO [14,15]), although recent works in the same or similar compounds suggest a 3D anisotropic behavior [16–22].

Here we study the anisotropy and dimensionality of high-quality 112 single crystals through measurements of the conductivity induced by superconducting fluctuations above T_c, $\Delta\sigma$. Fluctuation effects are also a powerful tool to determine other fundamental superconducting parameters, such as the coherence lengths or the critical fields [23,24], and are even sensitive to the multiband electronic structure [25–27]. The experiments were performed with magnetic fields H up to 9 T applied both parallel and perpendicular to the FeAs (ab) layers. These field amplitudes are large enough to explore the so-called *finite-field* or *Prange* fluctuation regime [23,24] and to quench the unconventional behavior observed in IBS below $\sim$ 1 T, usually attributed to phase fluctuations [28] or to a T_c distribution [26,29]. To analyze the data the Gaussian Lawrence-Doniach (LD) approach for $\Delta\sigma$ (see Ref. [30]) is generalized here to the finite-field regime and to high reduced temperatures through the introduction of a total-energy cutoff [31]. These data are complemented with measurements in another single crystal of the fluctuation-induced magnetization around T_c, ΔM. This observable is proportional to the effective superconducting volume fraction and confirms the bulk nature of the superconductivity in these materials. It also provides an important consistency check of the results.

Details of the crystal growth and characterization are presented in Sec. II, the measurements and analysis of $\Delta\sigma$ and ΔM in Secs. III and IV, respectively, the discussion of the results in Sec. V, and the conclusions in Sec. VI.

II. CRYSTAL GROWTH AND CHARACTERIZATION

The composition of the single crystals used in the experiments is $Ca_{1-x}La_xFe_{1-y}Ni_yAs_2$ with $x = 0.17 - 0.20$ and $y = 0.044(3)$. The partial substitution of Fe by Ni (or Co) improves the superconducting properties and sharpens the superconducting transition [8,32], which is essential to study critical phenomena around T_c. The crystals were grown by a self-flux method. The precursor materials CaAs, LaAs, FeAs, and NiAs were grinded with a molar ratio 3.7 : 0.3 : 0.95 : 0.05. The mixed powder was then pressed into a pellet, loaded into an Al_2O_3 crucible, and sealed into a quartz tube. The ampoule was heated to 1180 °C, slowly cooled down to 950 °C, and then to room temperature. After cracking the melted pellet, shining platelike single crystals with typical size $1\times1\times0.05$ mm^3 could be obtained. A thorough description may be seen in Ref. [33].

The stoichiometry of the three crystals used in the experiments (crystals 6, 9, and 11) was checked by energy-dispersive x-ray spectroscopy (EDX), performed with a Zeiss FE-SEM Ultra Plus system. EDX spectra were taken at five different points in each crystal (some examples are presented in Fig. 1). The average stoichiometry is presented in Table I, where the number in parentheses represents the standard deviation. The

*j.mosqueira@usc.es

 ©2017 American Physical Society

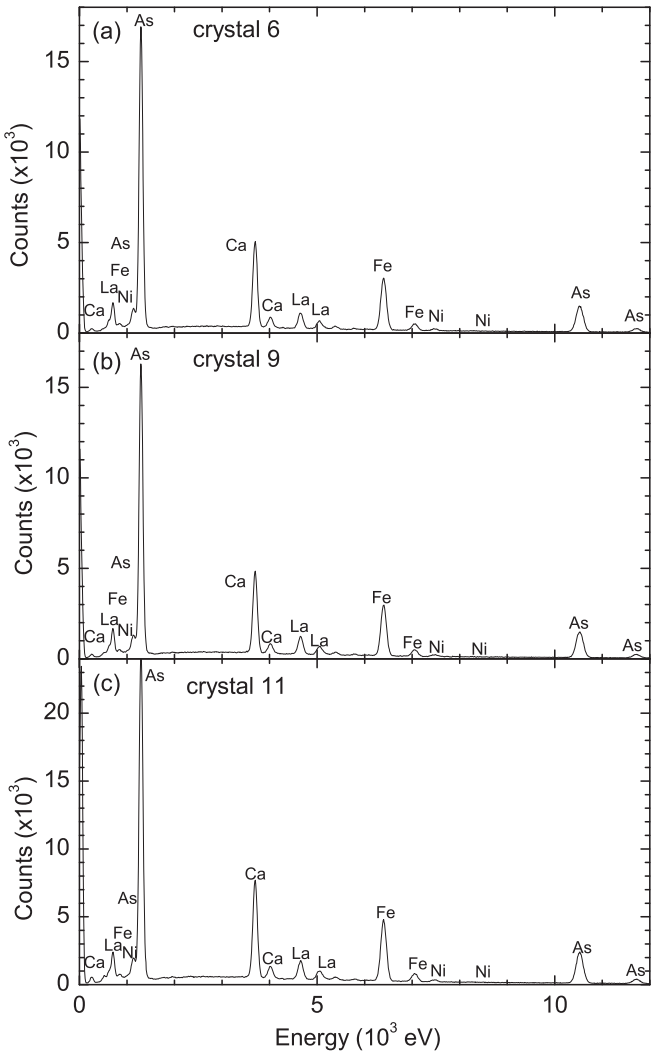

FIG. 1. Examples of EDX spectrum measured in the studied crystals.

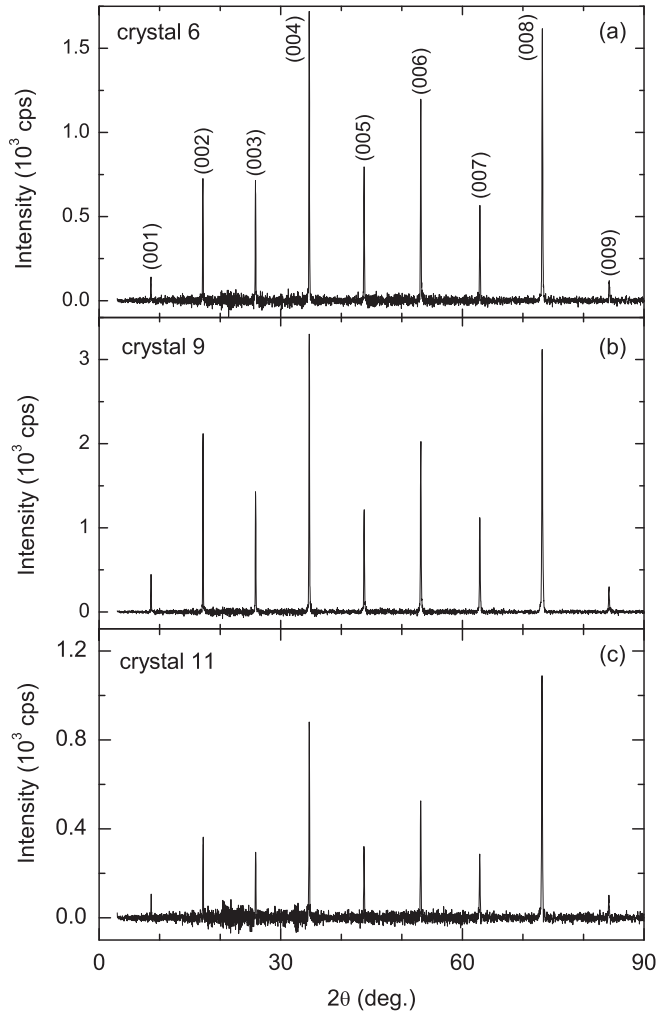

FIG. 2. XRD pattern of the studied crystals (already corrected for a background contribution).

differences from crystal to crystal in the average La content are slightly beyond the deviation, which will be useful to explore the dependence of superconducting parameters on the La doping level.

The crystallographic structure was studied by x-ray diffraction (XRD) by using a Rigaku MiniFlex II diffractometer with a Cu target. The $\theta - 2\theta$ patterns (see Fig. 2) present only (00l) reflections, which indicates the excellent structural quality of the crystals. The resulting c-axis lattice parameter (that is the same as the FeAs layer interdistance, s) is about 10.34 Å (see Table I), in agreement with data in the literature for crystals with a similar composition [2].

TABLE I. Average composition and interlayer distance of the studied samples, as follows from EDX and XRD.

Crystal	Composition					s
no.	Ca	La	Fe	Ni	As	(Å)
6	0.829(5)	0.172(2)	0.925(8)	0.044(3)	2.030(7)	10.336(1)
9	0.802(4)	0.199(7)	0.921(3)	0.044(2)	2.034(6)	10.343(1)
11	0.833(5)	0.176(3)	0.950(7)	0.045(3)	1.996(7)	10.348(1)

III. PARACONDUCTIVITY AND MAGNETOCONDUCTIVITY INDUCED BY FLUCTUATIONS

A. Experimental details and results

The resistivity along the ab layers, ρ, was measured in crystals 6 and 9 with a Quantum Design Physical Property Measurement System (PPMS) by using a four-wire technique with 1 mA excitation current at 71 Hz. The $\rho(T)_H$ behavior around T_c for both $H \parallel ab$ and $H \perp ab$ is presented in Fig. 3. The T_c values (see Table II) were estimated from the midpoint of the resistive transition in absence of field. The slight difference may be attributed to the above-mentioned differences in the La content. The transition *half-widths*, estimated from the 50%–10% criterion (above 50% intrinsic fluctuation effects also contribute to the transition widening), are around 0.6 K. This allowed to investigate fluctuation effects down to reduced temperatures $\varepsilon \equiv \ln(T/T_c)$ as low as 0.03. The resistivity rounding due to fluctuations extends

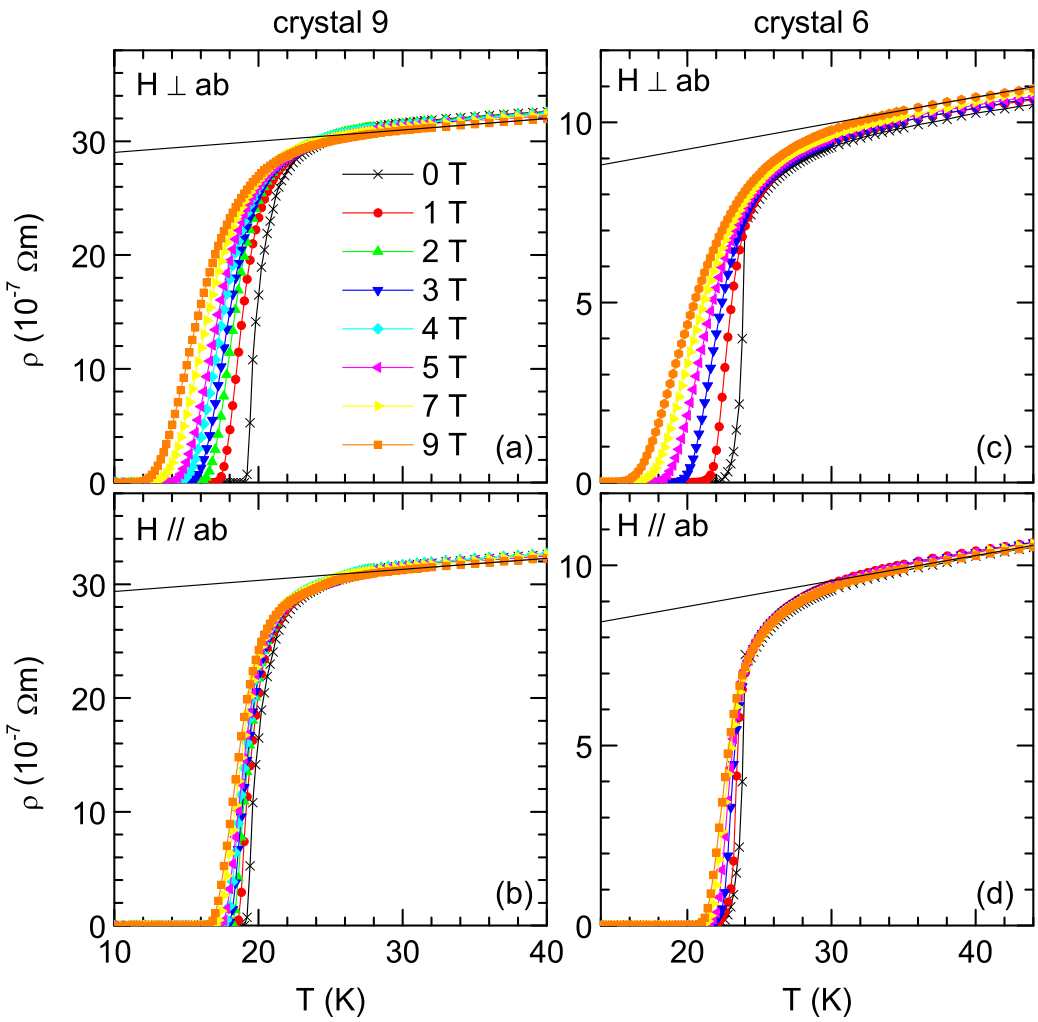

FIG. 3. T dependence of the resistivity around T_c of the studied crystals for both field orientations. The lines are examples (for $\mu_0 H = 9$ T) of the background contribution, as determined by a linear fit above 35 K, where fluctuation effects are expected to be negligible.

in both samples up to ~30 K ($\varepsilon \approx 0.4$) and is larger in amplitude than in other IBS, with a similar T_c and normal-state resistivity [29,34]. The Aslamazov-Larkin (AL) model for three-dimensional (3D) anisotropic superconductors predicts that $\Delta\sigma \propto \xi_c^{-1}(0)$ [23,24], where $\xi_c(0)$ is the c-axis coherence length amplitude. Thus, the enhanced fluctuation effects in 112-IBS is a first indication that these materials present a smaller $\xi_c(0)$, and may present a quasi-2D behavior if it is smaller than the FeAs interlayer distance. This seems to be the case in view of the almost inappreciable $T_c(H)$ shift for $H \parallel ab$, mainly in crystal 6.

TABLE II. Superconducting parameters of the studied crystals obtained from the analysis of fluctuation effects in the indicated observable.

Crystal no.	Obs.	T_c (K)	$\xi_c(0)$ (Å)	$\xi_{ab}(0)$ (Å)	r	γ
6	$\Delta\sigma$	23.9	0.65	19.3	0.016	29.7
9	$\Delta\sigma$	19.9	3.8	32.7	0.55	8.5
11	ΔM	21.8	1.9	27.0	0.13	14

B. Analysis of fluctuation effects above T_c

The fluctuation contribution to the conductivity $\Delta\sigma(T)_H$ was obtained from $\rho(T)_H$ through $\Delta\sigma(T)_H = 1/\rho(T)_H - 1/\rho_B(T)_H$, where the background resistivity $\rho_B(T)_H$ was obtained for each field by a linear fit from 35 to 40 K, above the onset of fluctuation effects. The upper limit was chosen to avoid a subtle change in the $\rho(T)_H$ behavior at higher temperatures, qualitatively similar to the one observed well above T_c in the other 112 compounds and attributed to magnetic/structural phase transitions [8].

1. Crystal no. 9

The resulting $\Delta\sigma(T)_H$ for this crystal is presented in Fig. 4. These data are first analyzed in terms of the Gaussian 3D-anisotropic Ginzburg-Landau (GL) approach developed in Ref. [29], which includes a cutoff in the energy of the fluctuation modes [31] and is valid beyond the zero-field limit:

$$\Delta\sigma_{3D} = \frac{e^2}{32\hbar\pi\xi_c(0)}\sqrt{\frac{2}{h}}\int_0^{\sqrt{\frac{c-\varepsilon}{2h}}} dx \times\left[\psi^1\left(\frac{\varepsilon+h}{2h}+x^2\right)-\psi^1\left(\frac{c+h}{2h}+x^2\right)\right]. \quad (1)$$

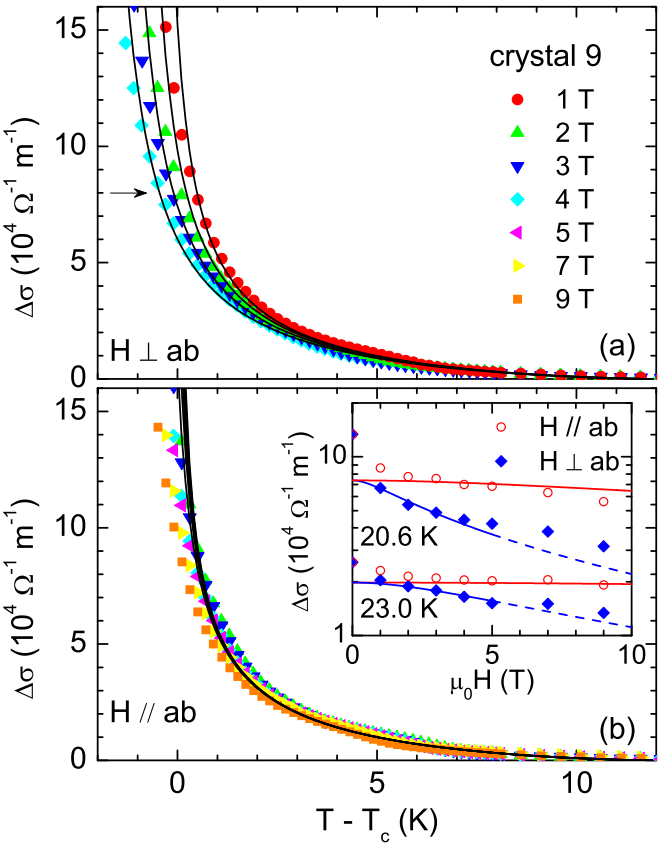

FIG. 4. Analysis of the results for crystal 9. (a) T dependence of $\Delta\sigma$ for $H \perp ab$. The lines are the best fit of Eq. (1) to the data up to the $\Delta\sigma$ value indicated by the arrow. (b) T dependence of $\Delta\sigma$ for $H \parallel ab$. Inset: H dependence for different temperatures above T_c. The lines in the main panel and in the inset were evaluated by using in Eq. (1) the superconducting parameters obtained in (a). See the main text for details.

Here ψ^1 is the first derivative of the digamma function, e is the electron charge, $\hbar$ is the reduced Planck constant, $h = H/H_{c2}(0)$ is the reduced magnetic field, $H_{c2}(0)$ is the upper critical field linearly extrapolated to $T = 0$ K (H_{c2}^c when $H \perp ab$, and H_{c2}^{ab} when $H//ab$), and c is the cutoff constant [31] that corresponds to the ε value for the onset of fluctuation effects. As in this crystal $\Delta\sigma$ is found to vanish at $T_{\text{onset}} - T_c \approx 12$ K, we approximated $c = \ln(T_{\text{onset}}/T_c) \approx 0.47$. Equation (1) is valid up to reduced magnetic fields of the order of $h \sim c/2 \approx 0.2$ (see Ref. [29]). As expected, in the zero-field limit ($h \ll \varepsilon$) and in absence of cutoff ($c \to \infty$) it reduces to the conventional 3D-AL expression [29].

The analysis for $H \perp ab$ is presented in Fig. 4(a). The lines are the best fit of Eq. (1) to the data obtained under magnetic fields from 1 to 4 T and up to $\Delta\sigma = 8\times10^4\ (\Omega\,\text{m})^{-1}$ (indicated by an arrow). We have checked that extending the fitting region above this $\Delta\sigma$ value increases significantly the root-mean-square deviation (RMSD). Then, this $\Delta\sigma$ limit may be associated to the onset of the critical region, where fluctuation effects are so large that the Gaussian approximation is no longer valid and Eq. (1) is not applicable. In what concerns the magnetic field range, data obtained with $\mu_0 H \geqslant 5$ T were excluded because they considerably worsened the fit quality. In view of the $H_{c2}^c(0)$ value resulting from the analysis (see below), this may be associated to the limit of applicability of the theory. In turn, we excluded data below 1 T because in this region $\Delta\sigma(H)$ presents an anomalous upturn [see the inset in Fig. 4(b)], an effect already observed in other IBS and attributed to the possible presence of phase fluctuations [28] but also to a T_c distribution [26,29].

The values obtained for the two fitting parameters are $\xi_c(0) = 3.8$ Å and $\mu_0 H_{c2}^c(0) = 30.7$ T, which leads to an in-plane coherence length amplitude of $\xi_{ab}(0) = \sqrt{\phi_0/2\pi\mu_0 H_{c2}^c(0)} = 32.7$ Å. The corresponding anisotropy factor $\gamma = \xi_{ab}(0)/\xi_c(0)$ is as large as 8.5 but still consistent with the 3D behavior, because the LD parameter $r \equiv [2\xi_c(0)/s]^2$, which is associated to the reduced temperature for the 3D-2D crossover [23], is ~0.55, above the onset of fluctuation effects.

The analysis for $H \parallel ab$ is presented in Fig. 4(b), where the solid lines were obtained without free parameters, by using in Eq. (1) the above $\xi_c(0)$ value and $\mu_0 H_{c2}^{ab}(0) = \gamma\mu_0 H_{c2}^c(0) = 261$ T. The agreement with the experimental data is also excellent, which is an important consistency check of our results. For completeness, in the inset of Fig. 4(b) the H dependence of $\Delta\sigma$ is presented for both field orientations and for two temperatures above T_c. The lines were obtained by using in Eq. (1) the above superconducting parameters. The dashed line corresponds to $H \gtrsim 0.2 H_{c2}^c(0)$, where the theory is no longer applicable.

2. *Crystal no. 6*

The $\Delta\sigma$ behavior of this crystal is presented in Fig. 5. As it may be seen in the inset in (b), $\Delta\sigma$ presents a monotonous behavior when $H \to 0$ near T_c, suggesting that T_c inhomogeneities or phase fluctuations play a negligible role in this sample. A first comparison with the theory may be then done with the data obtained with $H = 0$. As it is shown in the inset in Fig. 5(a), the $\Delta\sigma(T, H = 0)$ amplitude is appreciably larger than the one predicted by the 3D approach by using the $\xi_c(0)$ value previously found in crystal 9, and $c = 0.37$ (according to the ε value at which $\Delta\sigma$ vanishes in crystal 6). A smaller $\xi_c(0)$ value (about 1 Å) leads to an acceptable agreement with the data but is inconsistent with a 3D behavior. (It would lead to $r \approx 0.04$, so that the system should behave as 2D in almost all the accessible ε range.) In turn, the conventional 2D-AL approach, $\Delta\sigma = e^2/16\hbar s\varepsilon$ (dotted line) where s is the FeAs layer interdistance, strongly overestimates the experimental $\Delta\sigma$. The agreement improves with the introduction of an energy cutoff, which leads to $\Delta\sigma = e^2(\varepsilon^{-1} - c^{-1})/16\hbar s$ (dot-dashed line, see below), but only at high reduced temperatures. This suggests that a intermediate-dimensionality LD approach is needed.

A LD expression for $\Delta\sigma$ under finite applied magnetic fields may be obtained by adapting Eq. (B.18) of Ref. [29] (giving the fluctuation-induced conductivity in 3D as a sum over the contributions of different Landau levels) to the quasi-2D case by introducing the appropriate out-of-plane spectrum of the fluctuations [30] (i.e., substituting $\omega_{k_z}^{3D} = \xi_c^2(0)k_z^2$ by $\omega_{k_z}^{LD} = r[1 - \cos(k_z s)]/2$) and taking into account the structural cutoff in the z direction through $|k_z| \leqslant \pi/s$. This

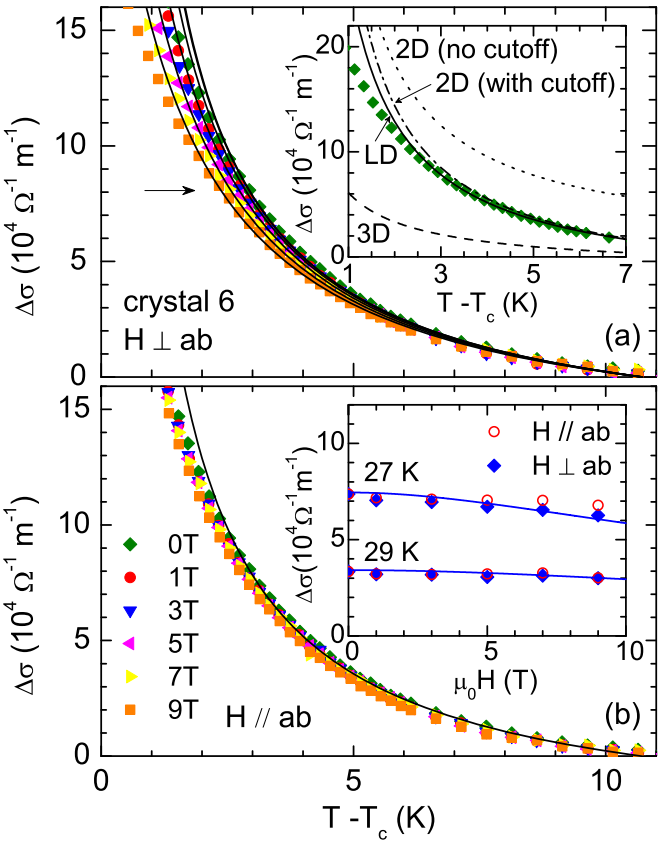

FIG. 5. Analysis of the results for crystal 6. (a) T dependence of $\Delta\sigma$ for $H \perp ab$. The lines are the best fit of Eq. (3) to the data up to the $\Delta\sigma$ value indicated by the arrow. Inset: Comparison of the $H = 0$ data with the 2D, 3D, and LD approaches (see the main text for details). (b) T dependence for $H \parallel ab$. The line was evaluated with the zero-field LD expression, Eq. (4), by using the r value obtained in (a). Inset: H dependence of $\Delta\sigma$ above T_c for both field orientations. The data for $H \parallel ab$ are almost H independent, as expected for a (quasi)-2D superconductor. The lines correspond to $H \perp ab$ and were evaluated by using in Eq. (3) the same parameters as in (a).

leads to

$$\Delta\sigma_{\rm LD} = \frac{e^2 h}{16\pi\hbar}\int_{-\pi/s}^{\pi/s} dk_z \sum_n \left[\varepsilon + h(2n+1) + \omega_{k_z}^{\rm LD}\right]^{-2}, \quad (2)$$

where the sum over Landau levels is to be performed up to $n_{\max} = (c-\varepsilon)/2h - 1$, resulting in

$$\Delta\sigma_{\rm LD} = \frac{e^2}{64\pi\hbar}\frac{1}{h}\int_{-\pi/s}^{\pi/s} dk_z \left[\psi^1\left(\frac{\varepsilon + h + \omega_{k_z}^{\rm LD}}{2h}\right) - \psi^1\left(\frac{c + h + \omega_{k_z}^{\rm LD}}{2h}\right)\right]. \quad (3)$$

In the low-field limit $h \ll \varepsilon$ this expression reduces to

$$\Delta\sigma_{\rm LD} = \frac{e^2}{16\hbar s}\left[\frac{1}{\sqrt{\varepsilon(\varepsilon+r)}} - \frac{1}{\sqrt{c(c+r)}}\right], \quad (4)$$

which in the absence of cutoff ($c \to \infty$) leads to the conventional LD paraconductivity [24].

The solid line in the inset of Fig. 5(a) is the best fit of Eq. (4) to the data obtained with $H = 0$ and up to $\Delta\sigma = 8\times10^4$ $(\Omega\,{\rm m})^{-1}$. By using a fitting region above this $\Delta\sigma$ value increases the RMSD significantly, so this $\Delta\sigma$ limit may be associated to the onset of the critical region where Eq. (4) is not applicable. The value obtained for the only free parameter is $r = 0.016$, which leads to $\xi_c(0) = 0.65$ Å, a value more than 1 order of magnitude smaller than the FeAs layer interdistance. The solid lines in the main panel of Fig. 5(a) are the best fit of Eq. (3) to the data obtained with $H \perp ab$ up to 9 T and up to the same limit, $\Delta\sigma = 8\times10^4$ $(\Omega\,{\rm m})^{-1}$. In this case we used the above r and c values, and obtained for the only free parameter $\mu_0 H_{c2}^c(0) = 88.1$ T. This value leads to $\xi_{ab}(0) = [\phi_0/2\pi\mu_0 H_{c2}^c(0)]^{1/2} = 19.3$ Å, and to an anisotropy factor as large as $\gamma = \xi_{ab}(0)/\xi_c(0) \approx 29.7$. This result is confirmed by the inappreciable effect of magnetic fields on $\Delta\sigma$ parallel to the ab layers, see Fig. 5(b).

IV. MAGNETIZATION INDUCED BY FLUCTUATIONS AROUND T_c

A. Experimental details and results

In order to confirm the above results we have performed additional measurements of the magnetization (M) induced by superconducting fluctuations in crystal no. 11. As commented above, this observable is proportional to the effective superconducting volume fraction and is suitable to confirm the bulk nature of the superconductivity in these compounds. The measurements were performed with a Quantum Design magnetometer (model MPMS-XL). The crystal was measured with H perpendicular to the ab layers. For that we used a quartz sample holder (0.3 cm in diameter, 22 cm in length) with a ~0.3-mm-wide groove perpendicular to its axis, into which the crystal was glued with GE varnish. Two plastic rods at the sample holder ends (~0.3 mm smaller than the sample space diameter) ensured that its alignment was better than 0.1°.

As a first magnetic characterization, in Fig. 6(a) is presented the temperature dependence of the low-field (0.3-mT) zero-field-cooled (ZFC) magnetic susceptibility, $\chi = M/H$. This measurement is corrected for demagnetizing effects by using as a demagnetizing factor $D = 0.86$, as it results by approximating the crystal shape by an ellipsoid. As it may be seen, χ is near the ideal shielding value of -1 just below the diamagnetic transition. $T_c \approx 21.8$ K was estimated as the temperature at which $d\chi/dT$ is maximum, and the transition width as $\Delta T_c = T(\chi = 0) - T_c \approx 1$ K that will allow us to study the fluctuation-induced magnetization in a wide temperature region above T_c (see below).

To measure the effect of superconducting fluctuations above T_c (which is in the 10^{-6} emu range), for each temperature we averaged eight independent measurements, from which we excluded the ones that deviate more than the standard deviation from the average value. The final resolution in magnetic moment m was in the $\sim 10^{-8}$ emu range. The as-measured $m(T)$ data around T_c are presented in Fig. 6(b). The solid (open) data points were obtained under ZFC (FC) conditions. As it is clearly seen, the reversible region extends a few degrees below T_c, allowing us to study the critical fluctuation regime. Just above the irreversibility temperature $m(T)$ presents an upturn that grows in amplitude with H. A very similar effect has also been observed in low-T_c alloys and has been attributed

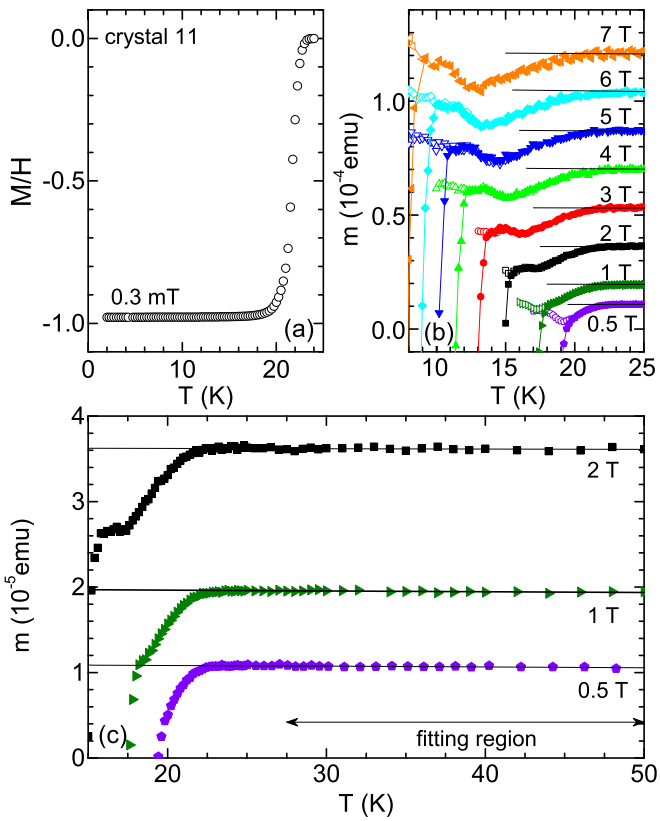

FIG. 6. (a) T dependence of the low-field (0.3 mT) ZFC magnetic susceptibility of crystal 11 (already corrected for demagnetizing effects). (b) Detail of the T dependence of the as-measured magnetic moment around T_c. Solid and open symbols were obtained under ZFC and FC conditions, respectively. The diamagnetism above T_c is unobservable in this scale. (c) Examples of the T dependence up to 50 K, where the normal-state backgrounds (lines) were determined by a linear fit in the indicated region.

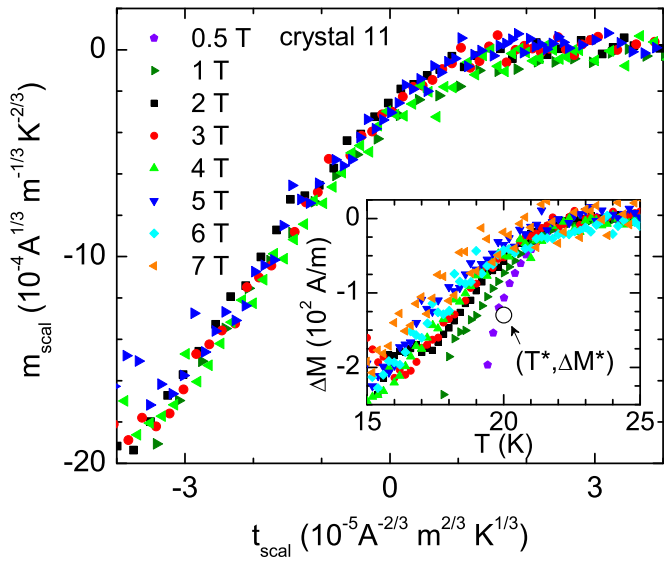

FIG. 7. 3D-GL scaling of the magnetization in the critical region. For clarity the noisy data for 6 T and 7 T were not included in the representation, but they are still consistent with the scaling. Inset: T dependence of the unscaled ΔM data around T_c. The circle is the prediction for the crossing point of 2D superconductors. See the main text for details.

to surface superconductivity [35]. In the following we will restrict the analysis of fluctuation effects to temperatures above this anomaly.

Some examples of the $m(T)_H$ behavior above T_c are presented in Fig. 6(c). In view of the almost constant temperature dependence, the background magnetic moment was determined by fitting a linear function, $m_B(T) = a + bT$, between 27.5 K (a temperature above which the rounding due to fluctuation effects is not appreciable) and 50 K. The temperature dependence around T_c of the magnetization induced by fluctuations $\Delta M = (m - m_B)/VH$ (where V is the crystal volume) is presented in the inset of Fig. 7.

B. Analysis in the critical region

A first direct analysis of the data may be done through Tesănović's approach for the magnetization in the critical region of 2D materials [36]. This model predicts that the $\Delta M(T)$ curves obtained under different H amplitudes cross at $\Delta M^* = -k_B T^*/\phi_0 s$, ΔM^* and T^* being the crossing point coordinates. In the case of crystal 11 the crossing occurs at much smaller ΔM amplitude (the the inset in Fig. 7), suggesting that the behavior in the critical region may be closer to that of a 3D superconductor. In this region, the 3D-GL approach in the lowest-Landau-level approximation predicts a scaling behavior in the variables [37,38],

$$m_{\text{scal}} \equiv \frac{\Delta M}{(HT)^{2/3}} \tag{5}$$

and

$$t_{\text{scal}} \equiv \frac{T - T_c(H)}{(HT)^{2/3}}, \tag{6}$$

where $T_c(H) = T_c[1 - H/H_{c2}^c(0)]$. This scaling was probed by using the above-determined T_c (see Table II) and $H_{c2}^c(0)$ as the only free parameter. The $H_{c2}^c(0)$ value that minimizes χ^2 with respect to a reference isofield data (4 T) is 45 T, although values between 40 and 50 T still lead to very similar scalings (the corresponding χ^2 are within $\sim$1%). As it may be seen in the main panel of Fig. 7, the 3D scaling is confirmed. The associated in-plane coherence length amplitude is $\xi_{ab}(0) = 27.0 \pm 1.5$ Å.

The 3D behavior in the critical region may still be consistent with a 2D behavior well above T_c if the transverse coherence length $\xi_c(T)$ shrinks to values well below the interlayer distance s. In fact, this is the case of a well-known quasi-2D superconductor like optimally doped $YBa_2Cu_3O_{7-\delta}$, which presents a 3D behavior in the critical region [39], and a 3D–2D transition in the Gaussian region well above T_c, at reduced temperatures around 0.1 [24].

C. Analysis in the Gaussian region

The fluctuation magnetic susceptibility in the Gaussian region above T_c is presented in Fig. 8. This measurement corresponds to $\mu_0 H = 1$ T. Lower applied magnetic fields lead to a proportionally lower signal-to-noise ratio, and for

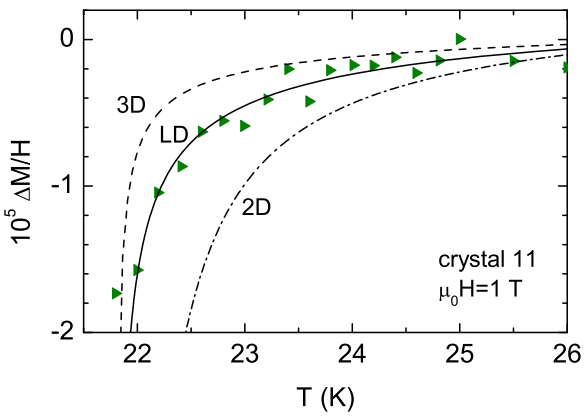

FIG. 8. Temperature dependence just above T_c of the fluctuation magnetic susceptibility obtained with $\mu_0 H = 1$ T. The solid line is the best fit of Eq. (7) above 22 K with r as the only free parameter. For comparison, the results for the 2D and 3D approaches are also included (see the main text for details).

fields above 1 T the superconducting quantum interference device sensitivity decreases significantly. In addition, 1 T is still much smaller than $\mu_0 H_{c2}^c(0) \approx 45$ T, so that the data are in the so-called low-field (or Schmidt) limit in which finite-field effects may be neglected. In this limit the LD model under a total-energy cutoff leads to [40]

$$\frac{\Delta M}{H} = -\frac{\pi \mu_0 k_B T \xi_{ab}^2(0)}{3\phi_0^2 s}\left[\frac{1}{\sqrt{\varepsilon(\varepsilon + r)}} - \frac{1}{\sqrt{c(c + r)}}\right]. \quad (7)$$

Here k_B is the Boltzmann constant, μ_0 the vacuum magnetic permeability, ϕ_0 the flux quantum, and $c = \ln(T_{\text{onset}}/T_c)$ the total-energy cutoff constant. When the LD parameter is $r \ll 1$ or $r \gg 1$, and in absence of cutoff ($c \to \infty$), this expression reduces to the classic results for the 2D or 3D limits, respectively. By using the T_c and $\xi_{ab}(0)$ values determined in the analysis of the critical region, and $c = 0.23$ as it corresponds to the above-determined $T_{\text{onset}} = 27.5$ K, the analysis depends only on r. The solid line in Fig. 8 is the best fit to the experimental data down to 22 K, which is very close to T_c. Below this temperature, the theory strongly overestimates the measured $\Delta M/H$ amplitude, which may be due to the onset of critical fluctuations. Note also that T_c inhomogeneities are expected to play a non-negligible role for temperatures below $T_c[1 + \Delta T_c/T_c - H/H_{c2}^c(0)]$, which is close to 22 K. The LD parameter resulting from the fit is $r = 0.13 \pm 0.03$, where the uncertainty comes from the one in the $H_{c2}^c(0)$ value. The r value is well below the onset reduced temperature, which confirms the quasi-2D nature of this material. The associated transverse coherence length is $\xi_c(0) = 1.9 \pm 0.2$ Å, that when combined with the above $\xi_{ab}(0)$ leads to an anisotropy factor as high as $\gamma = \xi_{ab}(0)/\xi_c(0) = 14 \pm 1$. The superconducting parameters for crystal 11 are also summarized in Table II. Just for completeness, the dot-dashed and dashed lines in Fig. 8 are the 2D and 3D limits of Eq. (7), evaluated by using $r = 0$ and 0.55, respectively. (This last reference value corresponds to the $\xi_c(0)$ value of the 3D crystal no. 9.)

V. DISCUSSION

A. Bulk nature of the superconductivity

The detailed characterization presented in Ref. [33] shows the bulk nature of the superconductivity in these compounds. The agreement of ΔM with the LD theoretical approach, and the fact that the resulting superconducting parameters are within the ones obtained from $\Delta\sigma$, further confirms this point, and also our conclusions about the high anisotropy and quasi-2D behavior of these materials. It is worth noting that $\Delta\sigma$ is also sensitive to the superconducting volume fraction; if it were small, $\Delta\sigma$ would be reduced roughly in the same proportion [40,41], and the analysis would be inconsistent. However, our results agree with the theoretical approaches by assuming a full superconducting volume fraction. Finally, the specific-heat jump at T_c (also directly proportional to the superconducting volume fraction) has been measured in crystals of a similar composition (Co doped instead of Ni doped) [8]. It is found $\Delta C_p/T_c = 6.7$ mJ/(mol Fe K^2), which follows the $\Delta C_p/T_c$ vs T_c scaling reported in Ref. [42] for different IBS.

B. T_c dependence of the superconducting parameters

As it may be seen in Fig. 9, the $\xi_{ab}(0)$ and $\xi_c(0)$ values obtained in the above analysis decrease as T_c increases. The dependence is more pronounced in the case of $\xi_c(0)$, and as a consequence the anisotropy factor presents a steep increase with T_c, reaching a value as high as ~30 in crystal 6. This sample presents the highest T_c and the smallest La doping level (0.172) of the studied samples. So it may be concluded that γ decreases for doping levels above the optimal one, which is expected to be about 0.15 [3,5]. Such a behavior is opposite to that observed in Ni-doped 122 single crystals, for which γ was found to increase upon increasing the Ni content above the optimal value [43].

The $\xi_c(0)$ reduction with the La doping level may be related to a weakening of the FeAs interlayer coupling. In fact, in the LD model of Josephson-coupled superconducting layers, the c-axis coherence length amplitude is related to the interlayer coupling constant Γ through $\xi_c(0) = s\sqrt{\Gamma}$ [44]. Then, we may assume that the La doping strongly affects the Josephson coupling between the FeAs layers. This is consistent with recent results on the electronic structure of $Ca_{0.85}La_{0.15}FeAs_2$, where it is concluded that *the Ca-La layers not only supply carriers but also tune the coupling between the As chains and the FeAs superconducting layers* [45].

C. Comparison with the anisotropy factors in other IBS

To our knowledge, the γ values found here (especially that of crystal 6) are among the largest ever reported in IBS. For instance, 1111 compounds present $\gamma(T_c) \approx 6$–9 [17,46–48], very recent works on FeSe intercalated with Li-NH_3 and with $Li_{1-x}Fe_xOH$ reported $\gamma(T_c) \approx 15$ [49,50], and in highly overdoped $Ba(Fe_{1-x}Ni_x)_2As_2$ ($x = 0.1$) it was found that $\gamma(T_c) \approx 16$. In a recent work on the anisotropic properties of a crystal from the 112 family ($Ca_{1-x}La_xFe_{1-y}Co_yAs_2$ with $x = 0.2$ and $y = 0.02$), it is reported $\gamma \approx 5$ near T_c [51]. The difference with the much larger γ values obtained in our crystals could be attributed to the smaller doping level. In fact, while the La concentration is similar, the Co concentration

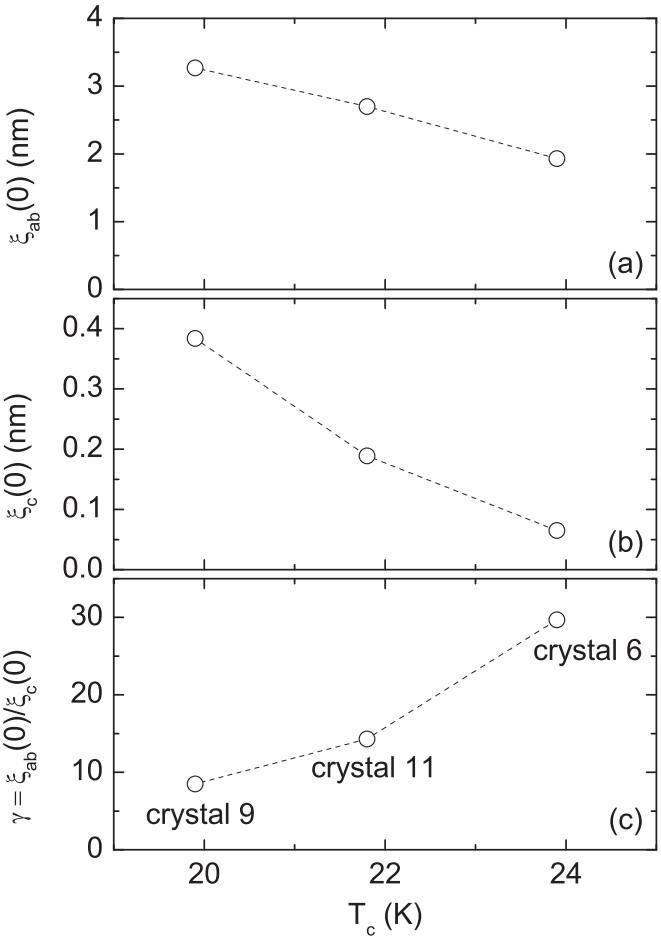

FIG. 9. T_c dependence of the coherence lengths and of the anisotropy factor of the studied samples.

is half that of Ni in our crystals, and also the Co valence is smaller than that of Ni.

It is worth noting that the majority of works in the literature obtain the anisotropy factor and coherence lengths from the shift of the resistive transition with H. However, in the present case, the large resistivity rounding due to quasi-2D fluctuations would introduce a large uncertainty (the result would be strongly dependent on the criterion used). In turn, procedures based on the analysis of the angular dependence of the magnetoresistivity around T_c in terms of the 3D-anisotropic GL approach [50–52] may not be applicable to quasi-2D superconductors.

D. Quasi-2D behavior

The $\xi_c(0)$ value resulted to be significantly smaller than the FeAs layer interdistance, $s = 10.34$ Å. In samples 6 and 11 this leads to a LD parameter well below the onset reduced temperature, so that a 3D-2D transition (a quasi-2D behavior) is observed at accessible reduced temperatures [53]. As commented on in the Introduction, early works suggest a 2D behavior in compounds with even smaller s values [11–15], but these results are not confirmed in more recent works in the same or similar compounds [16–22]. A 3D-2D transition has been recently proposed in 10-3-8 single crystals (with $s = 10.7$ Å) in Ref. [54], after the observation of a change in the critical exponent of $\Delta\sigma(H = 0)$ from $-1/2$ to -1. However, the $\xi_c(0)$ value found by these authors is close to $s/2$, which would be rather consistent with a 3D behavior up to high $\varepsilon \approx [2\xi_c(0)/s]^2 \approx 1$. It would be interesting, then, to check whether the seeming 2D critical exponent observed at $\varepsilon \approx 0.1$ in these compounds can be explained in terms of short-wavelength effects.

The combination of a large anisotropy and a large FeAs interdistance makes accessible the field scale above which 2D vortices would appear in the mixed state $\sim\phi_0/s^2\gamma^2$ (see, e.g., Ref. [23]). In fact, in crystal no. 6 this field would be only $\sim$2 T. This makes this compound a possible candidate to study 2D vortex physics in IBS.

VI. CONCLUSIONS

We have presented detailed measurements of the conductivity and magnetization induced by superconducting fluctuations near T_c of several high-quality single crystals of the 112 family, in particular, $Ca_{1-x}La_xFe_{1-y}Ni_yAs_2$ with $x = 0.17 - 0.20$ and $y = 0.044(3)$. As compared to the more studied 11, 111, 122, and 1111 families, this compound presents an extra As-As chain spacer-layer that increases the FeAs layer interdistance up to $s = 10.34$ Å, and it is expected to be strongly anisotropic. The data were then analyzed in terms of a generalization of the Lawrence-Doniach model to finite applied magnetic fields and high reduced temperatures through the introduction of a total-energy cutoff. This allowed a precise determination of fundamental superconducting parameters, like the in-plane and transverse coherence lengths. The resulting anisotropy factors are among the largest observed in IBS (up to $\sim$30 in the highest T_c crystal) and are directly correlated with the T_c value. This comes mainly from a significant $\xi_c(0)$ dependence on T_c, which may be related to a dependence of the interlayer coupling on the La doping level. In the higher T_c crystals $\xi_c(0)$ is much smaller than the FeAs layer interdistance s, leading to a 2D behavior at accessible reduced temperatures. In spite of this, the nonvanishing LD parameter is still consistent with a non-negligible coupling between adjacent FeAs layers, and then between the FeAs layers and the As chains, which seems to be a requisite for the existence of topological superconductivity in these compounds.

It would be interesting to extend our present results to a wider range of La- and Ni-doping levels, and to other IBS families with large FeAs interdistances, like 10-3-8 and 10-4-8 (also with intermediate As layers in the spacer layer) [55–57], 32522 [58], 42622 [59,60], $(Fe_2As_2)[Ca_{n+1}(Sc,Ti)_nO_y]$ (n = 3,4,5) [61], and 1144 (e.g., $CaKFe_4As_4$) [62].

ACKNOWLEDGMENTS

We thank Prof. Félix Vidal for valuable discussions and remarks on the manuscript. This work was supported by Project No. FIS2016-79109-P (AEI/FEDER, UE) and the Xunta de Galicia (Projects No. GPC2014/038 and No. AGRUP 2015/11). The work at IOP, CAS is supported by the NSFC (Projects No. 11374011 and No. 11674406), MOST of China (973 Projects No. 2012CB821400 and No. 2015CB921302), and the SPRP-B of CAS (Grant No. XDB07020300). H.L. is grateful for support from the Youth Innovation Promotion Association, CAS (Grant No. 2016004).

[1] For a recent review see, e.g., X. Chen, P. Dai, D. Feng, T. Xiang, and F.-C. Zhang, Nat. Sci. Rev. **1**, 371 (2014).

[2] N. Katayama, K. Kudo, S. Onari, T. Mizukami, K. Sugawara, Y. Sugiyama, Y. Kitahama, K. Iba, K. Fujimura, N. Nishimoto, M. Nohara, and H. Sawa, J. Phys. Soc. Jpn. **82**, 123702 (2013).

[3] K. Kudo, T. Mizukami, Y. Kitahama, D. Mitsuoka, K. Iba, K. Fujimura, N. Nishimoto, Y. Hiraoka, and M. Nohara, J. Phys. Soc. Jpn. **83**, 025001 (2014).

[4] K. Kudo, Y. Kitahama, K. Fujimura, T. Mizukami, H. Ota, and M. Nohara, J. Phys. Soc. Jpn. **83**, 093705 (2014).

[5] S. Kawasaki, T. Mabuchi, S. Maeda, T. Adachi, T. Mizukami, K. Kudo, M. Nohara, and G.-q. Zheng, Phys. Rev. B **92**, 180508 (2015).

[6] M. Y. Li, Z. T. Liu, W. Zhou, H. F. Yang, D. W. Shen, W. Li, J. Jiang, X. H. Niu, B. P. Xie, Y. Sun, C. C. Fan, Q. Yao, J. S. Liu, Z. X. Shi, and X. M. Xie, Phys. Rev. B **91**, 045112 (2015).

[7] X. Wu, S. Qin, Y. Liang, C. Le, H. Fan, and J. Hu, Phys. Rev. B **91**, 081111 (2015).

[8] S. Jiang, L. Liu, M. Schütt, A. M. Hallas, B. Shen, W. Tian, E. Emmanouilidou, A. Shi, G. M. Luke, Y. J. Uemura, R. M. Fernandes, and N. Ni, Phys. Rev. B **93**, 174513 (2016).

[9] S. Jiang, C. Liu, H. Cao, T. Birol, J. M. Allred, W. Tian, L. Liu, K. Cho, M. J. Krogstad, J. Ma, K. M. Taddei, M. A. Tanatar, M. Hoesch, R. Prozorov, S. Rosenkranz, Y. J. Uemura, G. Kotliar, and N. Ni, Phys. Rev. B **93**, 054522 (2016).

[10] Z. T. Liu, X. Z. Xing, M. Y. Li, W. Zhou, Y. Sun, C. C. Fan, H. F. Yang, J. S. Liu, Q. Yao, W. Li, Z. X. Shi, D. W. Shen, and Z. Wang, Appl. Phys. Lett. **109**, 042602 (2016).

[11] Y. J. Song, B. Kang, J.-S. Rhee, and Y. S. Kwon, Europhys. Lett. **97**, 47003 (2012).

[12] F. Rullier-Albenque, D. Colson, A. Forget, and H. Alloul, Phys. Rev. Lett. **109**, 187005 (2012).

[13] S. Pandya, S. Sherif, L. S. S. Chandra, and V. Ganesan, Supercond. Sci. Technol. **23**, 075015 (2010).

[14] I. Pallecchi, C. Fanciulli, M. Tropeano, A. Palenzona, M. Ferretti, A. Malagoli, A. Martinelli, I. Sheikin, M. Putti, and C. Ferdeghini, Phys. Rev. B **79**, 104515 (2009).

[15] S. Liu, W. Haiyun, and B. Gang, Phys. Lett. A **374**, 3529 (2010); S. L. Liu, B. Gang, and W. Haiyun, J. Supercond. Nov. Magn. **23**, 1563 (2010).

[16] M. Putti, I. Pallecchi, E. Bellingeri, M. R. Cimberle, M. Tropeano, C. Ferdeghini, A. Palenzona, C. Tarantini, A. Yamamoto, J. Jiang, J. Jaroszynski, F. Kametani, D. Abraimov, A. Polyanskii, J. D. Weiss, E. E. Hellstrom, A. Gurevich, D. C. Larbalestier, R. Jin, B. C. Sales, A. S. Sefat, M. A. McGuire, D. Mandrus, P. Cheng, Y. Jia, H. H. Wen, S. Lee, and C. B. Eom, Supercond. Sci. Technol. **23**, 034003 (2010).

[17] U. Welp, C. Chaparro, A. E. Koshelev, W. K. Kwok, A. Rydh, N. D. Zhigadlo, J. Karpinski, and S. Weyeneth, Phys. Rev. B **83**, 100513 (2011).

[18] S. Liu, W. Haiyun, and B. Gang, Solid State Commun. **151**, 1 (2011).

[19] S. Pandya, S. Sherif, L. S. S. Chandra, and V. Ganesan, Supercond. Sci. Technol. **24**, 045011 (2011).

[20] A. Ramos-Álvarez, J. Mosqueira, and F. Vidal, Phys. Rev. Lett. **115**, 139701 (2015).

[21] D. Ahmad, B. H. Min, W. J. Choi, S. Salem-Sugui, Jr., J. Mosqueira, and Y. S. Kwon, Supercond. Sci. Technol. **27**, 125006 (2014).

[22] D. Ahmad, W. J. Choi, Y. I. Seo, S. Seo, S. Lee, T. Park, J. Mosqueira, G. Gu, and Y. S. Kwon, New J. Phys. (to be published).

[23] M. Tinkham, *Introduction to Superconductivity* (McGraw-Hill, New York, 1996).

[24] A. I. Larkin and A. A. Varlamov, *Theory of Fluctuations in Superconductors* (Clarendon Press, Oxford, 2005).

[25] A. E. Koshelev and A. A. Varlamov, Supercond. Sci. Technol. **27**, 124001 (2014).

[26] A. Ramos-Álvarez, J. Mosqueira, F. Vidal, D. Hu, G. Chen, H. Luo, and S. Li, Phys. Rev. B **92**, 094508 (2015).

[27] K. Adachi and R. Ikeda, Phys. Rev. B **93**, 134503 (2016).

[28] G. Prando, A. Lascialfari, A. Rigamonti, L. Romanó, S. Sanna, M. Putti, and M. Tropeano, Phys. Rev. B **84**, 064507 (2011); L. Bossoni, L. Romanó, P. C. Canfield, and A. Lascialfari, J. Phys.: Condens. Matter **26**, 405703 (2014).

[29] R. I. Rey, C. Carballeira, J. Mosqueira, S. Salem-Sugui, Jr., A. D. Alvarenga, H.-Q. Luo, X.-Y. Lu, Y.-C. Chen, and F. Vidal, Supercond. Sci. Technol. **26**, 055004 (2013).

[30] S. Hikami and A. Larkin, Mod. Phys. Lett. B **02**, 693 (1988).

[31] F. Vidal, C. Carballeira, S. R. Currás, J. Mosqueira, M. V. Ramallo, J. A. Veira, and J. Viña, Europhys. Lett. **59**, 754 (2002).

[32] H. Yakita, H. Ogino, A. Sala, T. Okada, A. Yamamoto, K. Kishio, A. Iyo, H. Eisaki, and J. Shimoyama, Supercond. Sci. Technol. **28**, 065001 (2015).

[33] T. Xie, D. Gong, W. Zhang, Y. Gu, Z. Husges, D. Chen, Y. Liu, L. Hao, S. Meng, Z. Lu, S. Li, and H. Luo, arXiv:1705.11144.

[34] R. I. Rey, A. Ramos-Álvarez, C. Carballeira, J. Mosqueira, F. Vidal, S. Salem-Sugui, Jr., A. D. Alvarenga, R. Zhang, and H. Luo, Supercond. Sci. Technol. **27**, 075001 (2014).

[35] J. P. Gollub, M. R. Beasley, R. Callarotti, and M. Tinkham, Phys. Rev. B **7**, 3039 (1973).

[36] Z. Tešanović, L. Xing, L. Bulaevskii, Q. Li, and M. Suenaga, Phys. Rev. Lett. **69**, 3563 (1992).

[37] S. Ullah and A. T. Dorsey, Phys. Rev. Lett. **65**, 2066 (1990).

[38] S. Ullah and A. T. Dorsey, Phys. Rev. B **44**, 262 (1991).

[39] U. Welp, S. Fleshler, W. K. Kwok, R. A. Klemm, V. M. Vinokur, J. Downey, B. Veal, and G. W. Crabtree, Phys. Rev. Lett. **67**, 3180 (1991).

[40] R. I. Rey, C. Carballeira, J. M. Doval, J. Mosqueira, M. V. Ramallo, A. Ramos-Álvarez, D. Sóñora, J. A. Veira, J. C. Verde, and F. Vidal (unpublished).

[41] J. Maza and F. Vidal, Phys. Rev. B **43**, 10560 (1991).

[42] J. Zaanen, Phys. Rev. B **80**, 212502 (2009).

[43] A. Ramos-Álvarez, J. Mosqueira, F. Vidal, X. Lu, and H. Luo, Supercond. Sci. Technol. **28**, 075004 (2015).

[44] R. A. Klemm, A. Luther, and M. R. Beasley, Phys. Rev. B **12**, 877 (1975); M. V. Ramallo, A. Pomar, and F. Vidal, *ibid.* **54**, 4341 (1996).

[45] Z.-H. Liu, T. K. Kim, A. Sala, H. Ogino, J. Shimoyama, B. Bchner, and S. V. Borisenko, Appl. Phys. Lett. **106**, 052602 (2015).

[46] J. Jaroszynski, F. Hunte, L. Balicas, Y.-j. Jo, I. Raičević, A. Gurevich, D. C. Larbalestier, F. F. Balakirev, L. Fang, P. Cheng, Y. Jia, and H. H. Wen, Phys. Rev. B **78**, 174523 (2008).

[47] H.-S. Lee, M. Bartkowiak, J.-H. Park, J.-Y. Lee, J.-Y. Kim, N.-H. Sung, B. K. Cho, C.-U. Jung, J. S. Kim, and H.-J. Lee, Phys. Rev. B **80**, 144512 (2009).

[48] J. Karpinski, N. Zhigadlo, S. Katrych, Z. Bukowski, P. Moll, S. Weyeneth, H. Keller, R. Puzniak, M. Tortello, D. Daghero, R. Gonnelli, I. Maggio-Aprile, Y. Fasano, Ø. Fischer, K. Rogacki, and B. Batlogg, Physica C **469**, 370 (2009).
[49] S. Sun, S. Wang, R. Yu, and H. Lei, arXiv:1705.03301 .
[50] X. Yi, C. Wang, Q. Tang, T. Peng, Y. Qiu, J. Xu, H. Sun, Y. Luo, and B. Yu, Supercond. Sci. Technol. **29**, 105015 (2016).
[51] X. Xing, W. Zhou, N. Zhou, F. Yuan, Y. Pan, H. Zhao, X. Xu, and Z. Shi, Supercond. Sci. Technol. **29**, 055005 (2016).
[52] F. F. Yuan, Y. Sun, W. Zhou, X. Zhou, Q. P. Ding, K. Iida, R. Hühne, L. Schultz, T. Tamegai, and Z. X. Shi, Appl. Phys. Lett. **107**, 012602 (2015).
[53] It is interesting to mention the fact that materials with smaller s values, like $BaFe_{2-x}(Ni,Co)_xAs_2$, may still present 2D spin excitations and 3D (anisotropic) low-energy excitations within the FeAs plane. See, e.g., M. D. Lumsden, A. D. Christianson, D. Parshall, M. B. Stone, S. E. Nagler, G. J. MacDougall, H. A. Mook, K. Lokshin, T. Egami, D. L. Abernathy, E. A. Goremychkin, R. Osborn, M. A. McGuire, A. S. Sefat, R. Jin, B. C. Sales, and D. Mandrus, Phys. Rev. Lett. **102**, 107005 (2009); H. Luo, M. Wang, C. Zhang, X. Lu, L.-P. Regnault, R. Zhang, S. Li, J. Hu, and P. Dai, *ibid.* **111**, 107006 (2013).
[54] D. Ahmad, Y. I. Seo, W. J. Choi, and Y. S. Kwon, Supercond. Sci. Technol. **30**, 025009 (2017).
[55] S. Kakiya, K. Kudo, Y. Nishikubo, K. Oku, E. Nishibori, H. Sawa, T. Yamamoto, T. Nozaka, and M. Nohara, J. Phys. Soc. Jpn. **80**, 093704 (2011).
[56] C. Löhnert, T. Stürzer, M. Tegel, R. Frankovsky, G. Friederichs, and D. Johrendt, Angew. Chem. Int. Ed. **50**, 9195 (2011).
[57] N. Ni, J. M. Allred, B. C. Chan, and R. J. Cava, Proc. Natl. Acad. Sci. USA **108**, E1019 (2011).
[58] X. Zhu, F. Han, G. Mu, B. Zeng, P. Cheng, B. Shen, and H.-H. Wen, Phys. Rev. B **79**, 024516 (2009).
[59] H. Ogino, Y. Matsumura, Y. Katsura, K. Ushiyama, S. Horii, K. Kishio, and J. Shimoyama, Supercond. Sci. Technol. **22**, 075008 (2009).
[60] X. Zhu, F. Han, G. Mu, P. Cheng, B. Shen, B. Zeng, and H.-H. Wen, Phys. Rev. B **79**, 220512 (2009).
[61] H. Ogino, S. Sato, K. Kishio, J. Shimoyama, T. Tohei, and Y. Ikuhara, Appl. Phys. Lett. **97**, 072506 (2010).
[62] A. Iyo, K. Kawashima, T. Kinjo, T. Nishio, S. Ishida, H. Fujihisa, Y. Gotoh, K. Kihou, H. Eisaki, and Y. Yoshida, J. Am. Chem. Soc. **138**, 3410 (2016).